

# Code Verification exercise for 2D Poiseuille flow with non-Newtonian fluid

Stefano Lovato\*, Guilherme Vaz†, Serge Toxopeus†, Geert Keetels\*, Just Settels†

\*Delft University of Technology, Delft/Netherlands. † MARIN, Wageningen/Netherlands.  
s.l.lovato@tudelft.nl

## 1 Introduction

Safe navigation in port and waterways is ensured by setting a minimum distance between the ship's keel and the bottom, known as the under keel clearance (UKC). However, in ports situated at the estuary, the bottom is often covered by a layer of mud. Under these circumstances, the UKC is no longer unequivocally determined and the prediction of ship's manoeuvring behaviour becomes more challenging. Understanding the ships' behaviour in presence of mud layers is necessary both to improve safety during navigation and to optimize dredging operations in the interest of reducing the associated costs.

Model-scale experiments were done to link mud properties and ship's manoeuvrability (Delefortrie et al. (2005)). The large number of parameters to be addressed and the complex time dependent non-Newtonian behaviour of mud made very difficult to apply model-scale results to full-scale. CFD approach seems to be a good choice to overcome these obstacles (Toorman et al. (2015)).

The Newtonian model is widely used as constitutive equation for many fluids, such as water and air. However, it is not suitable to represent the flow behaviour of fluid mud<sup>1</sup>, which acts like a solid at low stress levels, but starts to flow when the stress exceeds a critical value, the yield stress,  $\tau_0$  (see Figure 1). Rheological measurements (e.g., Wurpts (2005)) have revealed that the Herschel-Bulkley model (Herschel and Bulkley (1926)) is appropriate to represent the flow behaviour of fluid mud. Thus, this non-Newtonian model has been implemented in a viscous-flow multiphase open-source code ReFRESKO ([www.refresco.org](http://www.refresco.org)).

The procedure and results of a Code Verification exercise are presented in this paper for the case of steady, laminar, two-dimensional Poiseuille flow with Herschel-Bulkley fluid.

## 2 A non-Newtonian constitutive equation for fluid mud: the Herschel-Bulkley model

The deviatoric stress tensor  $\boldsymbol{\tau}$  obeys the following constitutive equation for Herschel-Bulkley fluids:

$$\begin{cases} \boldsymbol{\tau} = 2 \left( \frac{\tau_0}{|\dot{\boldsymbol{\gamma}}|} + K |\dot{\boldsymbol{\gamma}}|^{n-1} \right) \mathbf{D}, & \tau_0 \leq |\boldsymbol{\tau}|, \\ \mathbf{D} = 0, & |\boldsymbol{\tau}| < \tau_0, \end{cases} \quad (1)$$

where  $\mathbf{D} = \frac{1}{2}(\nabla \mathbf{u} + \nabla \mathbf{u}^T)$  is the rate of strain tensor,  $\tau_0 [Pa]$  is the yield stress which represents the initial stress below which the fluid behaves as solid,  $K [Pa \cdot s^n]$  is the consistency parameter,  $|\boldsymbol{\tau}| = \sqrt{2\tau_{ij}\tau_{ij}}$  and  $|\dot{\boldsymbol{\gamma}}| = \sqrt{2D_{ij}D_{ij}}$  are the second invariant of the shear stress and rate of strain tensor respectively, which in some way are representative of the magnitude of the respective tensor. The parameter  $n$  is called flow index because it characterizes the flow behaviour of the fluid.

<sup>1</sup>The definition of fluid mud is not univocal. Here fluid mud is referred to as intermediate state between "black water", which has Newtonian flow characteristics, and consolidated mud, which behaves more like as an visco-elastic material.

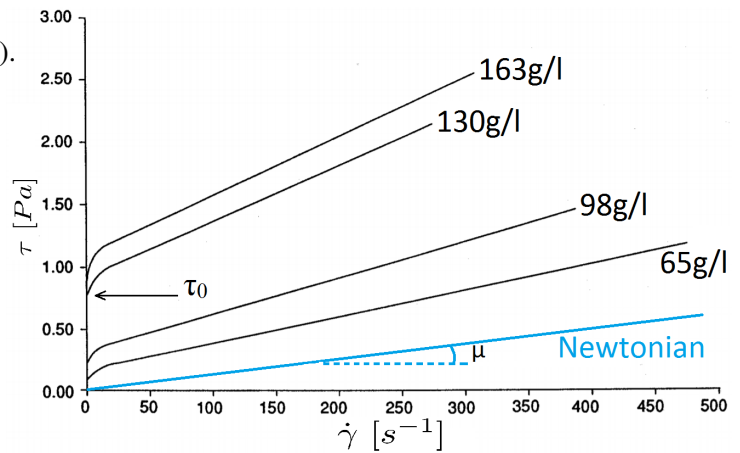
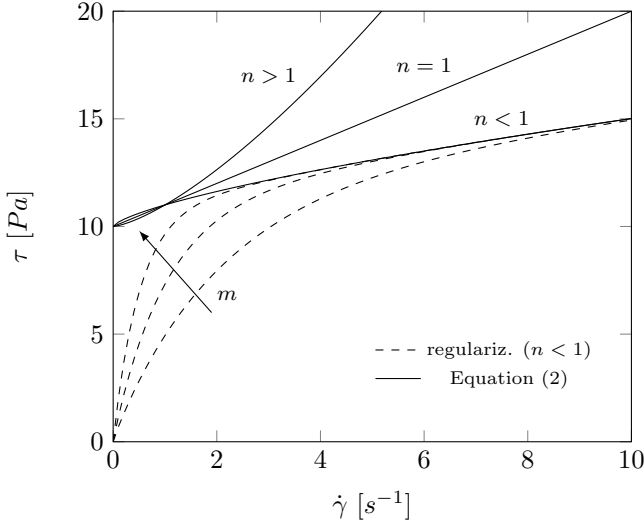


Fig. 1: Shear stress/Shear rate flow curves for different mud concentrations. In blue is shown the Newtonian model. Picture adapted from Whitehouse (2000).



**Fig. 2:** Shear stress versus shear rate for  $\tau_0 = 10 [Pa]$ ,  $K = 1 [Pa \cdot s^n]$  and different values of the flow index  $n$ . The Papanastasiou regularization is plotted varying the parameter  $m$ .

To circumvent this issue there are mainly two solution methods (Saramito et al. (2017)): the augmented Lagrangian algorithm and the regularization approach. The second method has been adopted because of its relatively simple implementation. It consists in approximating the curve described by Eq.(1) by a single smooth curve (Figure 2). Among the several regularizations that have been proposed by different authors, the most widely used is the one proposed by Papanastasiou (1987), which yields

$$\boldsymbol{\tau} = 2 \left[ \frac{\tau_0}{|\dot{\boldsymbol{\gamma}}|} \left( 1 - e^{-m|\dot{\boldsymbol{\gamma}}|} \right) + K |\dot{\boldsymbol{\gamma}}|^{n-1} \right] \mathbf{D}. \quad (2)$$

The term in the square brackets can be seen as one non-constant viscosity, generally called *apparent viscosity*:

$$\mu_{app} = \frac{\tau_0}{|\dot{\boldsymbol{\gamma}}|} \left( 1 - e^{-m|\dot{\boldsymbol{\gamma}}|} \right) + K |\dot{\boldsymbol{\gamma}}|^{n-1}. \quad (3)$$

The main advantage of the regularization approach is that ReFRESKO was already developed to solve flows with non-constant viscosity<sup>2</sup>, therefore the solver algorithm does not require major modifications. The implementation of the apparent viscosity then becomes quite straightforward.

It can be demonstrated that as  $m \rightarrow \infty$  the Eq.(2) tends to Eq.(1) and the solution with the regularized model tends to the exact solution of the Herschel-Bulkley model. However, with large values of  $m$  the iterative solver might not converge. Hence, a good compromise between accurate representation of the Herschel-Bulkley model and convergence must be found, depending on the objective of the computation.

### 3 Two-dimensional Poiseuille laminar flow

Poiseuille flow is the pressure driven, incompressible, steady, unidirectional and laminar flow that takes place in a duct when the Reynolds number is in the laminar range. Let consider x-y Cartesian reference system with the origin at the bottom of the duct and x axis pointing in the flow direction. Then the velocity field is like  $\mathbf{u} = (u(y), 0, 0)$  and the momentum equations written in a Cartesian coordinate system reduce to only one equation in the x direction:

$$\frac{dp}{dx} = \frac{d\tau_{xy}}{dy} \quad (4)$$

where  $p$  is the pressure which incorporates also the gravity term. Imposing the no-slip condition at the walls, i.e.  $u(y) = 0$  at  $y = 0$  and  $y = H$ , where  $H$  is the height of the duct, the analytical solution of Eq.(4)

<sup>2</sup>Non-constant viscosity with Newtonian fluid occurs when using, for instance, the Volume of Fluid method for multiphase problems, or eddy turbulent viscosity in the RANS equations.

Depending on whether  $n < 1$  (shear-thinning behaviour) or  $n > 1$  (shear-thickening behaviour) the fluid displays different flow curves (Figure 2). Note that when  $n = 1$  and  $\tau_0 = 0$  the model reduces to the Newtonian model. In addition, when  $n = 1$ , the consistency parameter  $K$  has dimensions of dynamic viscosity.

#### 2.1 Regularization approach

From the constitutive equation (1) two regions can be distinguished: one, called *un-yielded* region, where  $|\boldsymbol{\tau}| < \tau_0$  and the fluid does not experience any shear deformation; the other, called *yielded* region, where  $\tau_0 \leq |\boldsymbol{\tau}|$  and the fluid deforms. These two regions are not known a priori, so the solver does not know whether apply the first or the second relation in the equation (1).

combined with Eq.(1) yields (Ferrás et al. (2012)):

$$u(y) = \begin{cases} \frac{n}{n+1} \left(-\frac{dp}{dx}/2K\right)^{1/n} [(H/2 - H_0)^{(n+1)/n} - (|y - H/2| - H_0)^{(n+1)/n}], & H_0 \leq |y - H/2| \\ \frac{n}{n+1} \left(-\frac{dp}{dx}/2K\right)^{1/n} (H/2 - H_0)^{(n+1)/n}, & |y - H/2| \leq H_0 \end{cases} \quad (5)$$

where  $\frac{dp}{dx} < 0$  is given as the flow is pressure driven,  $H_0 = \tau_0/|\frac{dp}{dx}|$  is the height of half portion of the unyielded region (i.e., the region where  $|\tau| < \tau_0$ ).

In contrast with Newtonian fluids, Poiseuille flows of Herschel-Bulkley fluids are characterized by two non-dimensional numbers, the generalized Reynolds and Bingham numbers, defined respectively as

$$Re^* = \rho \frac{\bar{U}^{2-n} L^n}{K}, \quad Bi^* = \frac{\tau_0}{K(\bar{U}/L)^n} \quad (6)$$

where  $\bar{U}$  is the reference velocity,  $\rho$  is the fluid density and  $L$  is the reference length of the flow. In case of Poiseuille flow  $L$  is defined as the duct height and  $\bar{U}$  is the average velocity along the cross section. The Bingham number represents the non-dimensional yield stress. When  $n = 1$  and  $Bi^* = 0$ , the Newtonian case is retrieved. Note that when Poiseuille flow is in laminar regime the Reynolds number is irrelevant.

#### 4 Discretization error estimation

Performing a Code Verification exercise (which must be distinguished from Solution Verification and Validation) aims to check that (Eça et al. (2016)):

- the discretization error tends to zero as the grid reference spacing  $h$  tends to zero<sup>3</sup>.
- the rate of convergence  $p$  of the discretization error with the grid refinement tends to the order of the scheme adopted for the computations.

The *discretization error* is the difference between the exact solution of the original differential equation,  $\phi_{exact}$ , and the solution of the discretized equation,  $\phi_h$ , on a grid  $h$ . The other two components of numerical errors, the iterative and round-off error, must be kept as low as possible in order to have the best possible estimation of the discretization error. The iterative error can be neglected by dropping the solution residuals by at least three or four order of magnitude, whereas the round-off error is negligible as nowadays almost every computer uses double precision number format.

Although Eq.(5) is theoretically the exact solution, the use of the regularized approach in place of the original Herschel-Bulkley model makes it no longer appropriate for the estimation of discretization error. Thus, the exact solution has been computed numerically by solving Eq.(4), combined with the regularized Herschel-Bulkley model, Eq.(2). The equations have been discretized with the Finite Difference Method, dividing the height of the duct by approximately  $10^5$  points, a very large number of points compared to the finest grid used for the grid refinement study. For this reason, this solution is still referred to as “exact” even though it was computed numerically.

#### 5 Computational setup

The computation was set up to solve (steady) 2D computations. The duct considered for the grid refinement study has a length that is twice the height and has been discretized with Cartesian uniform grids having  $\frac{h_x}{h_y} = 1.5$ , where  $h_x$  and  $h_y$  are the cell size in the  $x$  and  $y$  direction respectively (see Figure 3). The coarsest grid, consisting of 24 cells, is systematically refined six times, halving both  $h_x$  and  $h_y$ , for a total of seven grids. Dividing  $h_x$  and  $h_y$  by the same factor is of utmost importance to preserve geometrical similarity between the grids.

The exact velocity profile is imposed at the inlet boundary. Fixed pressure and the no-slip condition are imposed at the outlet and wall boundaries respectively. The boundary conditions for both velocity and pressure are summarized in Table 1. The calculations on the seven grids were conducted for several combinations of Bingham number,  $Bi^*$ , and flow index,  $n$ . The regularization parameter,  $m$ , was set equal to 10 [s] for all the cases to facilitate iterative convergence.

<sup>3</sup>for unsteady problems also time refinement should be performed

Boundary conditions			
Inlet	Outlet	Wall	Side
$\mathbf{u} = \mathbf{u}_{exact}(y)$	$\nabla \mathbf{u} \cdot \mathbf{n} = \mathbf{0}$	$\mathbf{u} = \mathbf{0}$	$\nabla \mathbf{u} \cdot \mathbf{n} = \mathbf{0}$
$\frac{\partial p}{\partial n} = 0$	$p = const.$	$\frac{\partial p}{\partial n} = 0$	$\frac{\partial p}{\partial n} = 0$

**Table 1:** Boundary conditions for velocity and pressure on the computational domain

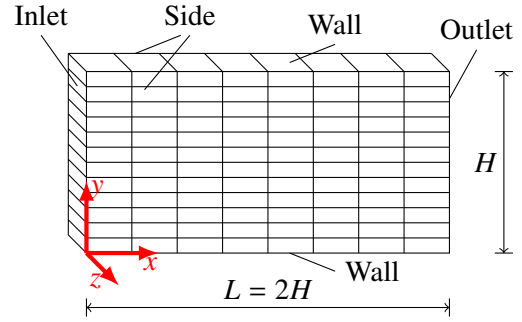


**Fig. 3:** Example of computational domain with 96 cells.

## 6 Results and discussion

Figure 4 shows how the iterative convergence of velocity along the  $x$  direction is influenced by  $Bi^*$  and  $n$  on the grid  $64 \times 96$ , which has an intermediate resolution. As a convergence criteria, the iterative solution was considered to be converged when the infinity norm of all the residuals was less than  $10^{-11}$ . Note that the least amount of iterations to find the converged solution are required for  $Bi^* = 0$ .

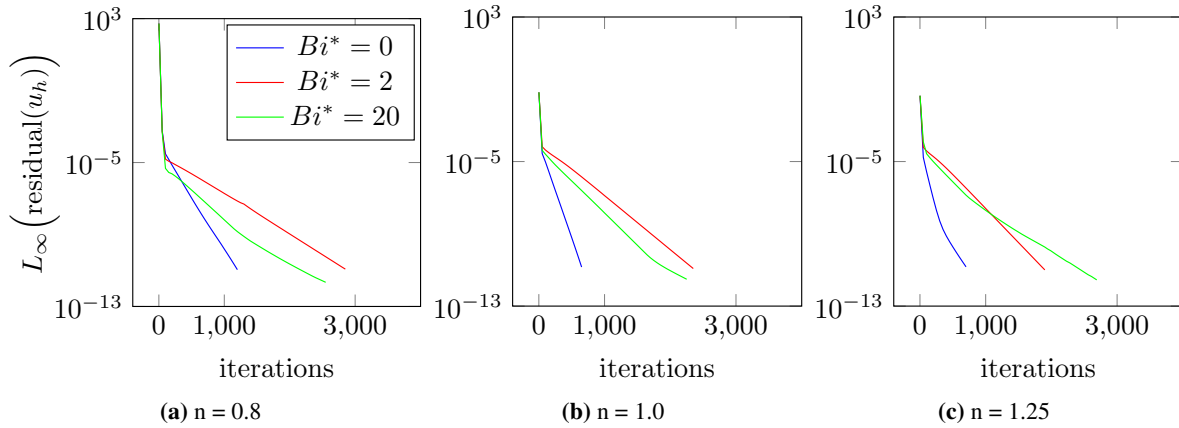


**Fig. 4:** Infinity norm of the velocity residuals in the  $x$  direction for the nine test cases.

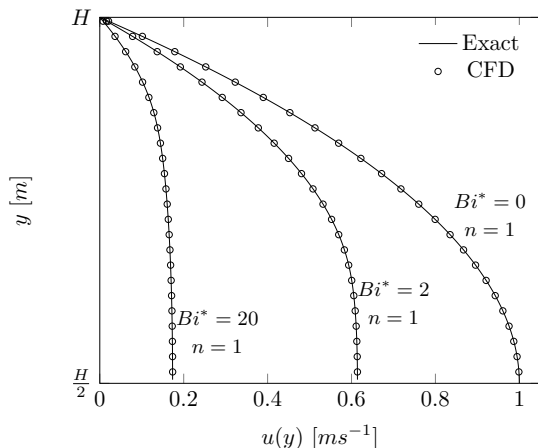


**Fig. 5:** Velocity profiles obtained with ReFRESCO and exact solution for different  $Bi^*$ . The duct has  $L = 20H$  and was discretized with a grid  $640 \times 96$ .

As additional verification, the velocity profile on a duct having length  $L = 20H$  was also computed, imposing this time an uniform velocity profile at the inlet boundary, providing no hints to the solver about the exact solution. The comparison between CFD solution and the exact solution reveals a very good agreement (Figure 5), with a maximum percentage error<sup>4</sup> below 0.2%.

The results of the grid refinement study are presented in Figure 6, showing the discretization errors of the velocity. As expected, the curves of discretization error converge to second order (i.e., converge to the line having slope  $p = 2$ ) as the grid spacing  $h_i/h_1$  tends to 1, with  $h_1$  the grid spacing of the finest grid. It can also be seen that, for higher  $Bi^*$ , finer grids are required to obtain the same accuracy as for  $Bi^* = 0$ . Similar results were found also for pressure and veloc-

<sup>4</sup>normalized with the velocity at  $y = H/2$

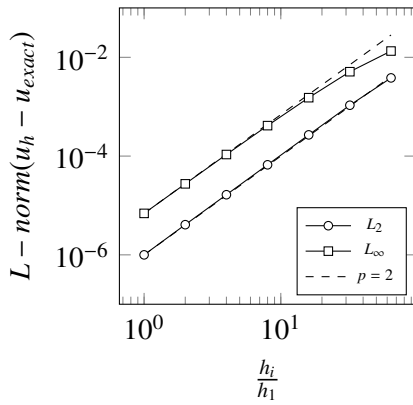
ity gradient. Other combinations of  $Bi^*$  and  $n$ , which are not reported here, were also tested, providing analogous results. The agreement of the observed order of convergence and the theoretical order of convergence demonstrates the correct implementation of the Herschel-Bulkley model.

Ultimately, it was found that when  $n \lesssim 0.7$ , or  $m \gtrsim 10^2$ , the solution did not converge anymore. If values beyond these thresholds need to be used in more realistic scenarios, (under-)relaxation methods should be considered to facilitate convergence.

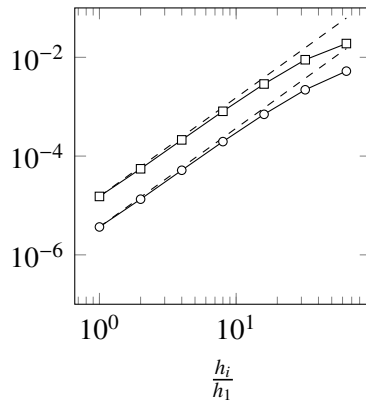
## 7 Conclusions

In this study, a code verification exercise was performed on the implementation of the Herschel-Bulkley model, which was adopted as non-Newtonian model to simulate the dynamics of fluid mud.

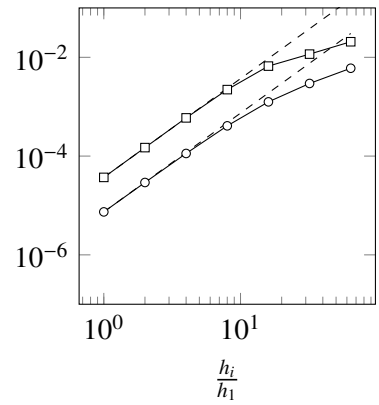
Results showed that the code is able to find an accurate solution (Figure 5), at least for a steady two-dimensional test case. In addition, this work highlighted that not only the discretization errors tends to zero as the grid is refined, but also that decreases with the expected second order (Figure 6). This seems to be a valid proof that the Herschel-Bulkley model is correctly implemented in ReFRESKO and thus that the code can be considered ready to solve problems with higher level of complexity (e.g., 3D domain, unsteady and multi-phase flows.).



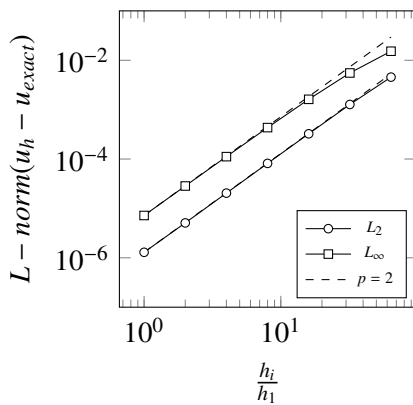
(a)  $n = 0.8, Bi^* = 0$



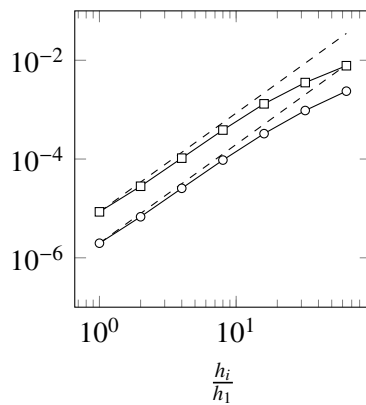
(b)  $n = 0.8, Bi^* = 2$



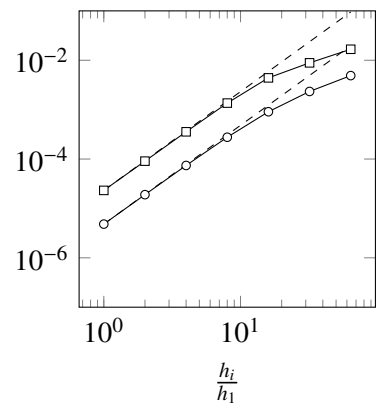
(c)  $n = 0.8, Bi^* = 20$



(d)  $n = 1.0, Bi^* = 0$  (Newtonian case)



(e)  $n = 1.0, Bi^* = 2$



(f)  $n = 1.0, Bi^* = 20$

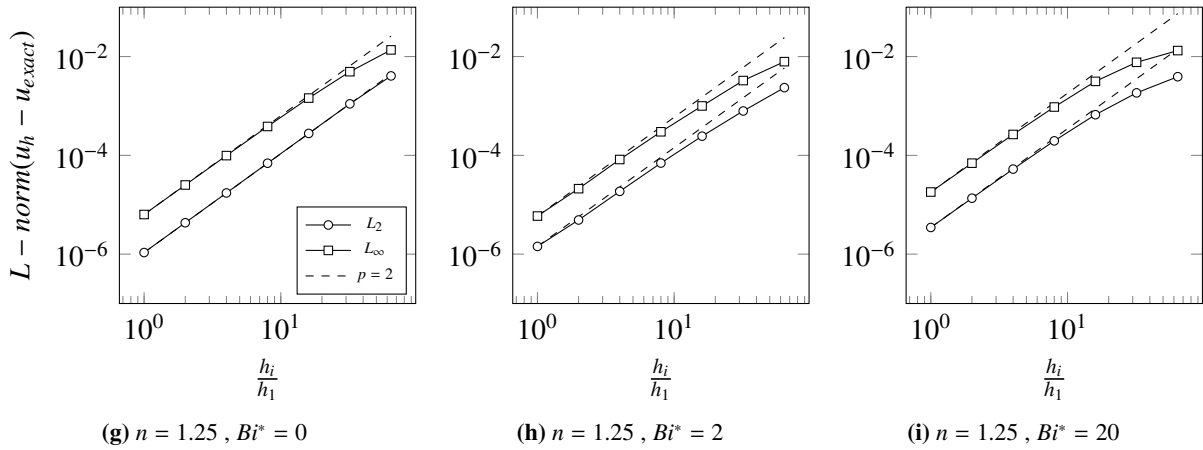


**Fig. 6:**  $L_2$  and  $L_\infty$  norm of the discretization error of the velocity for different combinations of  $Bi^*$  and  $n$ .  $u_h$  is the solution computed on the grid  $h$ .

## References

- G. Delefortrie, M. Vantorre, K. Eloot (2005). Modelling navigation in muddy areas through captive model tests. *Journal of marine science and technology*, 10(4), pp. 188-202.
- L. Eça, C.M. Klaij, G. Vaz, Hoekstra, F.S. Pereira (2016). On code verification of RANS solvers. *Journal of Computational Physics*, vol. 310, pp. 418 - 439.
- L.L. Ferrás, J.M. Nóbrega and F.T. Pinho (2012). Analytical solutions for Newtonian and inelastic non-Newtonian flows with wall slip. *Journal of Non-Newtonian Fluid Mechanics*, 175-176, 76-88.
- W.H.Herschel, R. Bulkley (1926). Konsistenzmessungen von Gummi-Benzllösungen, *Kolloid Zeitschrift*, 39:291-300.
- T.C. Papanastasiou (1987). Flows of materials with yield. *Journal of Rheology*, vol. 31, pp. 385.
- P. Saramito, A. Wachs (2017). Progress in numerical simulation of yield stress fluid flows. *Rheol Acta* (2017) 56 : 211 – 230.
- F. Stern, R. Wilson, V., H. W. Coleman, and E. G. Paterson. Comprehensive Approach to Verification and Validation of CFD Simulations - Part 1: Methodology and Procedures, *Journal of Fluids Engineering*, 2001, 123: pp. 793-802.
- E. A. Toorman, I. Vandebeek, M. Liste-Munoz, M. Heredia, I. Rocabado, J. Vanlede, G. Delefortrie, M. Vantorre, Y. Meersschaut(2015). Drag on an object towed through a fluid mud layer: CFD versus experiment. *International conference on cohesive sediment transport processes*, Abstracts, pp. 114-115.
- R. Whitehouse (2000). *Dynamics of Estuarine Muds: A Manual for Practical Applications*, p. 31
- R. Wurpts (2005). 15 Years Experience with Fluid Mud: Definition of the Nautical Bottom with Rheological Parameters. *Terra et Aqua* number 99, pp. 22-32.